Evaluation of NaCl and MgCl2 heat exchange fluids in a deep binary geothermal system in a sedimentary halite formation

Kayla R Moore (ummoor37@myumanitoba.ca)
University of Manitoba https://orcid.org/0000-0003-1718-3205
Hartmut M. Holländer
University of Manitoba

Research

Keywords: geothermal, thermal conductivity, halite, heat exchange fluid

Posted Date: December 29th, 2020

DOI: https://doi.org/10.21203/rs.3.rs-29544/v3

Version of Record: A version of this preprint was published at Geothermal Energy on February 27th, 2021.
See the published version at https://doi.org/10.1186/s40517-021-00190-3.

Evaluation of NaCl and $MgCl_2$ heat exchange fluids in a deep binary geothermal system in a sedimentary halite formation

Kayla R. Moore[1] and Hartmut M. Holländer[1]

[1] Department of Civil Engineering, University of Manitoba, Winnipeg, MB R3T 5V6

Corresponding author: Kayla Moore (ummoor37@myumanitoba.ca)

Abstract

Halite formations are attractive geothermal reservoirs due to their high heat conductivity, resulting in higher temperatures than other formations at similar depths. However, halite formations are highly reactive with undersaturated water. An understanding of the geochemical reactions that occur within halite-saturated formation waters can inform decision making regarding well construction, prevention of well clogging, formation dissolution, and thermal short-circuiting. Batch reaction and numerical 3-D flow and equilibrium reactive transport modeling were used to characterize the produced NaCl-brine in a well targeting a halite-saturated formation. The potential for inhibition of precipitation and dissolution using an $MgCl_2$-brine and NaCl+$MgCl_2$-brine were also investigated. Within the injection well for an NaCl-brine, with heating from 70 to 120°C, the solubility of halite decreases resulting in the potential dissolution of 0.479 mol kg^{-1} halite at the formation. Cooling from 120 to 100°C in the production well results in precipitation of 0.196 mol kg^{-1} halite as well as anhydrite. Introduction of $MgCl_2$, resulting in a common Cl^- ion, into the heat exchange brine resulted in a decreased potential for dissolution by 0.290 mol kg^{-1} halite within the formation, as well as decreased precipitation within the production well, compared to the NaCl-brine. The halite solubility was altered by changes in pressure up to 0.045 mol kg^{-1}. This indicates

that designing and monitoring the composition of heat exchange fluids in highly saline environments is an important component in geothermal project design.

Keywords: geothermal; thermal conductivity; halite; heat exchange fluid

1 Introduction

Deep geothermal systems can be used to produce electricity and have the potential to become a renewable baseload power source (Jain et al., 2015). Geothermal systems require adequate temperature, natural or engineered permeability, and a heat exchange fluid. Enhanced geothermal systems (EGS) are geothermal systems where hot rock is available, but the permeability or fluid saturation are created. Investigations into EGS for electricity production are underway in Canada and abroad, e.g. (Ferguson and Grasby, 2014; Grasby et al., 2012; Hadgu et al., 2016; Ledésert and Hébert, 2012; Limberger et al., 2018; Majorowicz and Moore, 2014). The Western Canadian Sedimentary Basin (WCSB) and Williston Basin in the Canadian Prairies have the potential for sedimentary geothermal energy production (Jacek and Stephen, 2010; Majorowicz and Moore, 2014; Manz, 2011; Walsh, 2013). However, due to the high cost of drilling, development has been limited.

One method for reducing drilling depth, and therefore cost, is to target thermal anomalies. In low-temperature formations (<200°C), conduction is the main process of heat transport (Scheck-Wenderoth et al., 2014). Due to the high thermal conductivity of halite, the tops of salt formations are associated with warm thermal anomalies, with higher temperatures than other rocks at similar depths (Petersen and Lerche, 1995). Daniilidis and Herber (2017) modeled a 40% increase in energy extraction and 25°C temperature increase in a salt formation. Therefore, halite

formations may be desirable as a geothermal target. However, saturated brine in the formation creates a challenge for geothermal operation (Moore and Holländer, 2020).

The geochemistry of produced fluid is the primary cause of technical issues in geothermal systems (Gunnlaugsson et al., 2014). The heat and flow requirements for deep geothermal systems have been extensively studied, e.g. Bujakowski et al. (2015), Plummer et al. (2016), and Xia et al. (2017). However, the geochemistry and geochemical reactions of heat exchange fluids, which can contain high mineral concentrations, remains a challenge (Frick et al., 2011; Gunnlaugsson et al., 2014). Formation waters are often the heat exchange fluid of choice in deep geothermal systems (Gunnlaugsson et al., 2014). However, since a halite formation, and likely overlying formations, would contain saturated saline brines, clogging due to mineral precipitation would be a major issue (Gunnlaugsson et al., 2014). Hesshaus et al. (2013) observed clogging due to precipitation of salt minerals between 655 and 1350 m in a 4000 m geothermal well in a sandstone formation. Borgia et al. (2012) simulated a CO_2 heat exchange fluid and found halite precipitation within the granite formation, which reduced permeability. At Bad Blumau, Austria, mineral scaling, corrosion, and chemical reactions between injection water and formations resulted in carbonate clogging within 5 days (Alt-Epping et al., 2013). When targeting a halite formation, we would, therefore, expect complex precipitation and dissolution.

Saturation, dissolution and precipitation of minerals within geothermal systems may be controlled by choice of heat exchange fluid. Salts from the evaporating sea, or evaporates, under ideal conditions, deposit in layers based on their solubility (Appelo and Postma, 2005). The following sequence of deposition should be expected: calcite ($CaCO_3$), dolomite ($CaCO_3 \cdot MgCO_3$), anhydrite ($CaSO_4$), halite (NaCl), sylvite (KCl), carnallite ($KCl \cdot MgCl_2 \cdot 6H_2O$) and bischofite ($MgCl_2 \cdot 6H_2O$). Therefore, bischofite is most likely to stay in solution. The common-

ion effect is the decrease in solubility of a precipitate resulting from a soluble compound with an ion in common with the precipitate. The expected effect of adding $MgCl_2$ to a solution is a decrease in halite solubility (Nishri et al., 1988). Therefore, to reduce the precipitation and dissolution of a halite reservoir, a designed heat exchange fluid is proposed.

Halite formations result in temperature anomalies that can benefit low-temperature geothermal systems. However, the geochemical technical issues in such a system are complex. Therefore, the objective of this work is to quantify geochemical reactions in a halite geothermal system to provide an understanding of dissolution and precipitation with the changes in temperature and pressure that occur in such a system. The geochemistry was examined in the injection and production wells, in the formation and at the surface. Inhibition of dissolution and precipitation was explored by introducing an $MgCl_2$-brine as the injected heat exchange fluid. Therefore, this work provides insight into the technical issues associated with the development of a geothermal doublet system in a halite formation, technical issues associated with fluid geochemistry, and a potential solution, in the form of an engineered heat exchange fluid.

2 Materials and Methods

The precipitation and dissolution in a geothermal system targeting a deep halite formation were investigated using reactive transport modeling. The conceptual model was based on a geothermal doublet in the Prairie Evaporite, a halite formation in the Williston Basin in the Canadian Prairies of Devonian age. The Prairie Evaporite has been identified as a potential geothermal target due to its high thermal conductivity e.g. Firoozy (2016).

Saturated NaCl-brine, representing a natural brine, as well as an inhibitory $MgCl_2$-brine and an $MgCl_2$-brine in equilibrium with the formation composition (NaCl+$MgCl_2$-brine) were evaluated as heat exchange fluids. Reactive transport modeling has been applied in geothermal

systems to investigate problems such as saline fluids in a granite system (Bächler and Kohl, 2005), precipitation in CO_2 heat exchange fluid systems (Alt-Epping et al., 2013; Borgia et al., 2012), precipitation at an acid-neutral fluid interface (Todaka et al., 2004) and to assess fluid pathways and geochemical reactions (Wanner et al., 2014). In this study, the composition of heat exchange fluid compositions in highly saline environments was investigated using PHREEQC Version 3 (Parkhurst and Appelo, 2013) a computer program designed to calculate a wide variety of aqueous geochemical calculations, including saturation-index calculations, as well as FEFLOW (Diersch, 2014) and piCHEM (Wissmeier, 2015) a finite element method (FEM) for calculating flow and transport in porous and fractured media.

2.1 Reservoir and thermal fluids

The values for temperature, pressure and geochemistry were based on the Prairie Evaporite. This formation is located within the Williston Basin, part of the larger Western Canadian Basin. The formation is dominantly halite with anhydrite and potash inclusions. The formation is of Devonian age (Bezys and McCabe, 1996). The thickness of the Prairie Evaporite ranges from 25 to 300 m (Grobe, 2000). Across western Canada, the thickness of overburden ranges from 200 m in northeastern Alberta, to 2300 m in central Alberta, 700 m in central Saskatchewan to 2700 m in southern Saskatchewan (Grobe, 2000), and approximately 1100 m at the Manitoba Saskatchewan border (TGI Williston Basin Working Group, 2008). High heat flow, up to 70 to 90 mW m^{-2} is expected in this region, resulting in temperatures of 80 to 130°C at a depth of 3.5 km (Majorowicz and Grasby, 2010). The estimated average porosity of the WCSB is 11.8% (Grasby et al., 2012); however, the porosity of halite is much lower, 2% (Winkler, 2011). The permeability of halite is very low; estimates range from $1x10^{-13}$ to $1x10^{-20}$ m^2 (Beauheim et al., 1999).

The composition of the Prairie Evaporite was provided by a salt solution mine located at Hargrave, Manitoba (Table 1). The chemical composition of this brine was used to calculate the chemical composition at other temperatures, assuming equilibrium with halite. Earl and Nahm (1981) assessed salt concentrations in the Williston Basin. They found that the solutions were saturated with halite, and often contain large amounts of calium and magnesium. At 2500 – 2700 m chloride levels of 200 g L^{-1} would ensure supersaturation at the bottomhole temperature (Earl and Nahm, 1981). The density of halite is 2323 g L^{-1}, and a saturated brine is expected to have a density of 1200 kg m^{-3} at atmospheric conditions.

Table 1: Concentrations of ions in a saturated NaCl-brine based on the fractions for the Prairie Evaporite. Provided by Christie (2015), as in Moore and Holländer (2017). Due to field measurements, some values may reach supersaturation.

	Unit	Prairie Evaporite
Temperature	°C	30
Na^+	mol kg^{-1}	8.46
Cl^-	mol kg^{-1}	9.71
Mg^{2+}	mol kg^{-1}	5.02×10^{-4}
K^+	mol kg^{-1}	1.78×10^{-2}
Ca^{2+}	mol kg^{-1}	2.59×10^{-2}
Fe^{3+}	mol kg^{-1}	2.72×10^{-6}
SO_4^{2-}	mol kg^{-1}	3.69×10^{-2}

2.2 Model Conceptualization

The concept for the geothermal setup is a 5 MW, EGS, binary, doublet system (Figure 1). The permeability in the area surrounding the wells is assumed to be stimulated using hydraulic fracturing. Hydraulic fracturing is effective in sedimentary geothermal reservoirs and is commonly used in oil and gas in the WCSB (Legarth et al., 2005). A flow rate of 6000 m^3 d^{-1} was used, based on literature values for hydraulic head and temperature values (Firoozy, 2016; Jain et al., 2015; Luo et al., 2014; Xia et al., 2017). The geothermal system is a low temperature (<150°C), low enthalpy (<800 kJ kg^{-1}), liquid dominated system (Axelsson and Gunnlaugsson, 2000). The operational time for the well is 30 years. A batch reaction model was used to complete an in-depth characterization of all minerals in the formation and a 3-D model was used to understand temporal aspects.

Three fluid compositions were considered for heat exchange fluids in the binary geothermal system. First, a NaCl-brine saturated at 10°C, based on the composition of the Prairie Evaporite, second a pure $MgCl_2$-brine saturated at 10°C, and third, a NaCl+$MgCl_2$-brine based on the composition of the formation in equilibrium with minerals found in the Prairie Evaporite saturated at 10°C. Temperatures were roughly based on those observed in binary geothermal systems (DiPippo, 2004). Initial fluid saturations are considered at 10°C, the lowest temperature expected in the flow system during storage. The injection temperature is 40°C. After traveling down the injection well, and upon entering the formation the temperature is 70°C. Temperature is initially a homogeneous 120°C throughout the halite formation. Within the production well the temperature is expected to cool to 100°C (Alt-Epping et al., 2013). At the ground surface, a minimum temperature of 10°C is considered. Solubility was calculated and compared at these temperatures. These values for injection and produced temperatures are conservative values which allow for heat loss in the wells.

Figure 1: Conceptual model with injection well, halite reservoir, production well, and surface conditions. Shown are the temperature conditions and flow rates. Also shown are the 4 intervals discussed in 2.3.1.

2.2.1 Temperature and Pressure Evaluations

The solubility of salts is dependent on pressure and temperature. The solubility of saturated halite and bischofite solutions were considered at the range of values expected in geothermal wells, 0.1 to 60 MPa, and 5 to 130°C (Figure 2). For both minerals, the solubility is more sensitive to changes in temperature than pressure. Therefore, the temperature was considered the main driver in solubility changes for the simulations. Dissolved bischofite reaches a maximum solubility as H_2O_{gas} becomes supersaturated.

Figure 2: Cl^- concentration in solution for halite and bischofite solutions in freshwater with changes in temperature and pressure from the Pitzer.dat from Moore and Holländer (2017)

2.3 Numerical Approach

2.3.1 Batch Reaction Calculations

The geothermal system geometry was simplified to points along a flow path, similar to the approach adopted by Alt-Epping et al. (2013) (Figure 1). The batch reactive transport simulations were conducted using PHREEQC 3 (Parkhurst and Appelo, 2013). The geothermal geometry is strongly simplified; however, geochemical data are examined. The flow of the fluid is discussed in 4 intervals: (1) the reactions within the heat exchange fluid as it descends and temperature and pressure increase; (2) the reactions between the heat exchange fluid and formation; (3) the

reactions within the heat exchange fluid as it ascends and temperature and pressure decrease; (4) the reactions that occur as a result of the extraction of heat at the surface.

Saturated NaCl, $MgCl_2$ and NaCl+$MgCl_2$-brines were evaluated as heat exchange fluids within the Prairie Evaporite. The heat exchange fluids are initially saturated at 10°C, reflecting average surface temperatures. Two fluids were based on the values in Table 1 saturated with halite for the NaCl-brine, and bischofite for the NaCl+$MgCl_2$-brines. The $MgCl_2$-brine was based on a pure water saturated with bischofite. First, the saturation of key minerals was considered as fluid warmed from 10°C to 70°C from the surface to the bottom of the injection well (interval 1); then 70°C to 120°C within the reservoir (interval 2). Next, the cooling phases were considered: first 120°C to 100°C within the extraction well (interval 3); then 100°C to 70°C and 10°C at the surface (interval 4). The concentrations of individual ions were calculated based on equilibrium with halite (SI = 0.0) throughout the process. The precipitation and dissolution of halite was estimated based on the concentration of sodium in the fluid. The effect of changes in pressure as the fluid moves up the production well was further explored, with pressures from 0.1 to 202 MPa evaluated for each heat exchange fluid composition, and temperatures of 100 and 120°C considered.

2.3.2 3-D Model Design

The model design consists of a binary geothermal reservoir, with a 300 m thick simulation domain (z-direction). A region 1200 m (x-direction) by 1000 m (y-direction) by 300 m (z-direction) was considered, with a cross-section occurring at the wellbore (Figure 3). Considering the top of the formation in plane with the well at (0, 0, 0) m, the injection well was located at (300, 0, 75) m and production well was located at (900, 0, 225) m. The distance between the wells was 618 m. The model domain was divided into 195,520 elements in 28 layers, with increased

discretization near the injection well. The pressure was hydrodynamic, assuming a depth of 3000 m.

Figure 3: 3-D model domain and boundaries for a binary geothermal doublet.

The simulation domain was considered a low permeability halite, enhanced by hydraulic fracturing. The model region was assumed to have been fractured, except for the outer 25 m of the model, which was assumed to be intact halite. Fractures were simulated as an equivalent porous matrix, which is acceptable for geothermal simulations at the reservoir scale (Jarrahi et al., 2019). The equivalent hydraulic conductivity (K_{fr}) and porosity (ε_{fr}) were estimated from Snow (1968):

$$K_{fr} = \frac{\rho \cdot g \cdot N \cdot b^3}{6\mu} \quad 2\text{-}1$$

$$\varepsilon_{fr} = 3Nbg \quad 2\text{-}2$$

where ρ (kg m^{-3}) is the fluid density, g (m s^{-2}) is the acceleration due to gravity, and μ (kg m^{-1} s^{-1}) is viscosity. A fracture density, N of 1 m^{-1} was assumed, with a range examined from 0.001 to 10 m^{-1} (Kalinina et al., 2014). The fracture aperture, b is assumed to be "partly open" with a value of 0.3 mm, examined at a range of 0.1 mm to 5 mm (Dehkordi et al., 2014). Assuming water density of 1200 kg m^{-3}, a viscosity of 2x10^{-4} kg m^{-1} s^{-1} and acceleration of gravity of 9.81 m s^{-2}, the density of 1 m^{-1} and aperture of 0.3 mm results in a K_{fr} of 2.65x10^{-4} m s^{-1}and ε_{fr} of 9x10^{-4}. The viscosity value was based on an NaCl brine at 70°C (Ozbek et al., 1977). The model was assumed to be anisotropic with hydraulic conductivity in the horizontal direction 10 times flow in the vertical direction.

The injection and production wells were simulated as Neumann condition well boundary types with a flow rate of 3000 $m^3\ day^{-1}$, which is half of the targeted flow rate, appropriate for a cross-section. A constant head boundary of 0 m was assigned to the top of the model, and the initial head was set at 0 m. Two heat exchange fluids were evaluated, NaCl and $MgCl_2$-brines saturated at 10°C and 0.1 MPa. Injection of the heat exchange fluids was simulated as a constant concentration at the injection well. No flow geochemical boundaries were used at the top, bottom and sides of the model. The initial geochemical composition of the formation fluid was assumed to be in equilibrium with the known composition of the Prairie Evaporite, saturated at formation pressure and temperature. An initial temperature of 120°C was used in the formation. The fluid was injected at 70°C. Mass transport parameters were set at: porosity 0.3, diffusion to 1 x $10^{-9}\ m^2\ s^{-1}$, longitudinal dispersivity 12 m, and transverse dispersivity 1.2 m. For heat transport, the volumetric heat capacity of fluid was 4.2 MJ $m^{-3}\ K^{-1}$, the volumetric heat capacity of solid was 2.52 MJ $m^{-3}\ K^{-1}$, the thermal conductivity of fluid 0.65 J $m^{-1}\ s^{-1}\ K^{-1}$ and the thermal conductivity of soil 5 J $m^{-1}\ s^{-1}\ K^{-1}$ (Firoozy, 2016). The volumetric heat capacity of fluid was chosen to one of pure water instead of the one of a saturated $MgCl_2$ (2.6 MJ $m^{-3}\ K^{-1}$ (Lach et al., 2017)) or NaCl brine (3.2 MJ $m^{-3}\ K^{-1}$ (Lach et al., 2017)). The composition of the brine will change with simulation time so that we decided on a larger value. According to Nalla et al. (2005), the smaller volumetric heat capacity of the fluid is likely to increase the temperature of the fluid, while decreasing the heat extracted from the fluid in the cycling of the system. Since the main focus of this work was mineral compositions, the impact is considered to be minimal.

2.3.3 3-D Model Sensitivity Analysis

An equivalent porous media approach was used to represent fractures within the 3-D model. This has been shown to work effectively; however, it is sensitive to the calibration of porosity and permeability (Jarrahi et al., 2019). Therefore, the sensitivity of the 3-D model to fracture aperture and density was analyzed (Table 2).

Fractures in deep geothermal systems develop perpendicular to the least stress (Fisher and Warpinski, 2012). This creates anisotropy. Flow in the horizontal direction is initially assumed to be 10 times flow in the vertical direction. Sensitivity is investigated for flow in the vertical direction 10 times flow in the horizontal direction.

Table 2 Values used for fracture densities from $1x10^{-3}$ to 10 m^{-1} and fracture apertures $1x10^{-4}$ to $5x10^{-3}$ m used to assess model sensitivity.

Character ID	N	B	ε_{fr}	K_{fr}
	m^{-1}	m	-	m s^{-1}
1	1	3×10^{-4}	9×10^{-4}	2.65×10^{-4}
2	10	5×10^{-3}	0.15	12.2
3	10	1×10^{-4}	3.0×10^{-3}	9.81×10^{-5}
4	1×10^{-3}	5×10^{-3}	1.5×10^{-6}	1.23×10^{-4}
5	1×10^{-3}	1×10^{-4}	3×10^{-7}	9.81×10^{-9}

2.4 Mathematical Representation

PHREEQC Version 3 (Parkhurst and Appelo, 2013) calculations were made using the Pitzer.dat, which is designed for use with high ionic strengths and high temperatures (Plummer et

al., 1988). PHREEQC reads a database file of thermodynamic data, which was used to calculate solubility and thermodynamic stability. The Pitzer.dat database was used due to its application to high salinity problems (Parkhurst and Appelo, 2013). Equilibrium values were used for the simulations, which have been observed at the reservoir scale (Fu et al., 2012).

FEFLOW (Diersch, 2014) uses a multidimensional FEM to solve the governing flow, mass and heat transport equations in porous and fractured media. The plug-in piCHEM (Wissmeier, 2015) which couples PHREEQC (Parkhurst and Appelo, 2013) with FEFLOW is used to solve reactive transport. Reactive transport reactions were calculated at equilibrium.

The flow of groundwater was calculated assuming a non-deforming media following (Garven, 1995) and limited deformation calculated by Jarrahi et al. (2019). The mass conservation equation of a saturated fluid is given as:

$$S_0 \frac{\partial h_0}{\partial t} + \nabla \cdot \vec{q} = Q \qquad 2\text{-}3$$

where S_0 is specific storage (m^{-1}), and Q is sinks and sources (s^{-1}). Saturated Darcy fluid flux $\vec{q}$ (m s^{-1}) in FEFLOW is defined as:

$$\vec{q} = -\boldsymbol{K} \cdot (\nabla h_0 + \chi \vec{e}) \qquad 2\text{-}4$$

where $\boldsymbol{K}$ (m s^{-1}) is the hydraulic conductivity tensor, h_0 (m) is the equivalent freshwater hydraulic head, e is the gravitational unit vector (1). The density ratio (χ) (-) in FELFOW describes the ratio between maximum and minimum density and is defined as:

$$\chi = \frac{\rho_s - \rho_0}{\rho_0} \qquad 2\text{-}5$$

where ρ_s (kg m^{-3}) is the saltwater density and ρ_0 (kg m^{-3}) is the freshwater density. For this work, a value of 0.2 was applied. The equivalent freshwater hydraulic head can be calculated as:

$$h_0 = (1 + \chi)h_s - \chi z \qquad 2\text{-}6$$

where h_s is the saltwater hydraulic head (m) and z is the elevation head (m).

Heat transfer at equilibrium between the solid and fluid phase can be described using Fourier's law as:

$$(\varepsilon\rho c + (1 - \varepsilon)\rho_m c_m)\frac{\partial T}{\partial t} + \rho c\vec{q} \cdot \nabla T - \nabla \cdot (\boldsymbol{\Lambda} \cdot \nabla T) = H_e - \rho c(T - T_0)Q \qquad 2\text{-}7$$

where ε is porosity (-), ρ is the mass density of the fluid (kg m^{-3}), c is specific heat capacity (m^2 s^{-2} K^{-1}), ρ_s is the mass density of the solid (kg m^{-3}), c_s is the specific heat capacity of solid (m^2 s^{-2} K^{-1}), T is temperature (K), T_0 is reference temperature (K), t is time (s), $\vec{q}$ is the Darcy velocity of fluid (m s^{-1}), $\boldsymbol{\Lambda}$ is the tensor of hydrodynamic thermodispersion (kg m s^{-3} K^{-1}) and Q is a sink/source term (s^{-1}).

Solute transport involves the complex, nonlinear interactions of ions, as well as the changes in density. The presence of undersaturated fluid within a matrix can cause dissolution, while supersaturated fluids result in precipitation. The coupling of geochemistry and flow using piCHEM assumes that aqueous phase flow can be represented by the transport of individual dissolved components. The governing equation used for solute transport is classic advection-diffusion/dispersion equation (Wissmeier, 2015):

$$\frac{\partial C_i}{\partial t} = -\nabla \cdot (\vec{q} C_i) + \nabla \cdot (\theta \boldsymbol{D} \nabla C_i) + S_C \quad \text{2-8}$$

where c_i (kg m^{-3}) is the concentration of solution species i, t is time (s), θ (m^3 m^{-3}) is the relative liquid phase saturation, $\boldsymbol{D}$ (m^2 s^{-1}) is the hydrodynamic dispersion tensor and S_C (kg m^{-3} s^{-1}) is a source-sink term. The liquid phase is composed of solution species according to (Wissmeier, 2015):

$$\theta = \frac{\sum_i n_i m_i}{\rho} \quad \text{2-9}$$

where n_i (mol m^3) is the volume of species i in a control volume with molar weight m_i (kg mol^{-1}). The phase mass balance is then (Wissmeier, 2015):

$$\frac{\partial \rho \theta}{\partial t} = -\nabla \cdot \rho \theta \vec{v} \quad \text{2-10}$$

where $\vec{v}$ (m s^{-1}) is the mass flow velocity of the liquid phase.

3 Results

Reactive transport modeling was used to evaluate the interaction between a halite formation, and three heat exchange fluids in a deep geothermal system. Potential mineral precipitates were evaluated for a saturated NaCl-brine, $MgCl_2$-brine and NaCl+$MgCl_2$-brine over temperature changes expected in the reservoir (Table 3, Table 4, Table 5).

Next, a 3-D reactive transport model was used for reservoir simulations to investigate the suitability of these fluids as heat exchange fluids in geothermal systems over 30 years. The

formation water was assumed to be saturated with halite and contained other trace minerals. Heat exchange fluids were assumed to be saturated with NaCl at 10°C and $MgCl_2$ at 10°C respectively.

3.1 Batch reaction chemical simulations

3.1.1 Potential Precipitation

When injecting a NaCl-brine into a deep geothermal well, within the injection well, the NaCl-brine becomes undersaturated with respect to halite (Table 3). Upon reaching the halite formation, dissolution of up to 0.479 mol kg^{-1} halite occurs to bring the solution to saturation. Note that this value is dependent on reactions approaching equilibrium values. The fluid then travels up the production well cooling from 120 to 100°C. This cooling results in precipitation of 0.196 mol kg^{-1} halite as well as anhydrite.

Within the injection well, the $MgCl_2$-brine becomes unsaturated with respect to halite (Table 4). After reaching the halite formation, dissolution of up to 0.189 mol kg^{-1} halite occurs to bring the solution to saturation. The fluid then travels up the production well cooling from 120 to 100°C. This cooling results in precipitation of 0.087 mol kg^{-1} halite.

Within the injection well the NaCl+$MgCl_2$-brine becomes unsaturated with respect to halite (Table 5). After reaching the halite formation, dissolution of up to 0.189 mol kg^{-1} halite occurs to bring the solution to saturation. The fluid then travels up the production well cooling from 120 to 100°C. This cooling results in precipitation of 0.088 mol L^{-1} halite as well as unmeasured amounts of anhydrite and bischofite.

The effect of changes in pressure from 0.1 to 202 MPa were evaluated. As pressure increases, the solubility of NaCl increases. For the NaCl-brine, pressure change from 0.1 to 202 MPa increased the solubility of the solution by 0.045 mol kg^{-1}. The $MgCl_2$ and NaCl+$MgCl_2$-

brines were less susceptible to pressure changes with a 0.0017 mol kg^{-1} increase in solubility from 0.1 to 30 MPa.

Table 3: NaCl heat exchange fluid composition and mineral saturation indices (SI) during heating and cooling processes as determined using PHREEQC 3 and Pitzer.dat. Bold numbers indicate saturation or supersaturation. Solutions is considered at equilibrium with halite.

			Heating (Injection)			Max	Cooling (Extraction)		
Mineral	Formula		10°C	40°C	70°C	120°C	100°C	70°C	10°C
Anhydrite	$CaSO_4$	SI	-0.46	-0.14	**0.10**	**0.33**	**0.26**	**0.10**	-0.46
Bischofite	$MgCl_2 * 6H_20$	SI	-6.58	-6.38	-6.20	-6.00	-6.07	-6.20	-6.58
Brucite	$Mg(OH)_2$	SI	-6.51	-6.48	-6.19	-5.84	-5.94	-6.19	-6.50
Carnallite	$KMgCl_3:6H_2O$	SI	-7.41	-7.63	-7.74	-7.80	-7.79	-7.74	-7.41
Glauberite	$Na_2Ca(SO_4)_2$	SI	-1.02	-0.71	-0.48	-0.27	-0.32	-0.48	-1.03
Goergeyite	$K_2Ca_5(SO_4)6H_2O$	SI	0.32	-1.54	-2.59	-3.47	-3.21	-2.60	**0.32**
Gypsum	$CaSO_4:2H_2O$	SI	-0.16	-0.22	-0.30	-0.51	-0.41	-0.30	-0.16
Halite	NaCl	SI	**0.00***	**0.00***	**0.00***	**0.00***	**0.00***	**0.00***	**0.00***
Kieserite	$MgSO_4: H_2O$	SI	-5.99	-5.64	-5.19	-4.42	-4.72	-5.16	-5.99
Polyhalite	$K_2MgCa_2(SO_4)_4 * 2H_2O$	SI	-8.82	-9.01	-9.73	-11.9	-10.9	-9.7	-8.82

Sylvite	KCl	SI	-1.98	-2.24	-2.42	-2.63	-2.56	-2.42	-1.98
pH			7.0	6.3	5.9	5.7	5.8	6.0	7.0
Ca	Ca^{2+}	mol kg^{-1}	2.59×10^{-2}	2.59×10^{-2}	2.59×10^{-2}	2.59×10^{-2}	2.59×10^{-2}	2.59×10^{-2}	2.59×10^{-2}
Cl	Cl^{-}	mol kg^{-1}	6.74	6.85	7.09	7.57	7.37	7.01	6.74
Fe	Fe^{3+}	mol kg^{-1}	2.76×10^{-6}	2.76×10^{-6}	2.76×10^{-6}	2.76×10^{-6}	2.76×10^{-6}	2.76×10^{-6}	2.76×10^{-6}
K	K^{+}	mol kg^{-1}	1.78×10^{-2}	1.78×10^{-2}	1.78×10^{-2}	1.78×10^{-2}	1.78×10^{-2}	1.78×10^{-2}	1.78×10^{-2}
Mg	Mg^{2+}	mol kg^{-1}	5.02×10^{-4}	5.02×10^{-4}	5.02×10^{-4}	5.02×10^{-4}	5.02×10^{-4}	5.02×10^{-4}	5.02×10^{-4}
Na	Na^{+}	mol kg^{-1}	5.47	5.58	5.81	6.29	6.10	5.82	5.47
S	SO_4^{2-}	mol kg^{-1}	3.69×10^{-2}	3.69×10^{-2}	3.69×10^{-2}	3.69×10^{-2}	2.856×10^{-2}	3.69×10^{-2}	3.69×10^{-2}
ΔHalite	Incremental	mol kg^{-1}	0	1.11×10^{-1}	2.39×10^{-1}	4.79×10^{-1}	-1.96×10^{-1}	-2.82×10^{-1}	-3.48×10^{-1}
ΔHalite	Total	mol kg^{-1}	0	1.11×10^{-1}	3.50×10^{-1}	8.29×10^{-1}	6.33×10^{-1}	3.51×10^{-1}	3.33×10^{-3}

Table 4: $MgCl_2$ heat exchange fluid composition and mineral saturation indices (SI) during heating and cooling processes as determined using PHREEQC 3 and Pitzer.dat. Bold numbers indicate saturation or supersaturation, * indicates equilibrium phase.

			Heating (Injection)			Max	Cooling (Extraction)		
Mineral	Formula		10°C	40°C	70°C	120°C	100°C	70°C	10°C
Bischofite	$MgCl_2 * 6H_20$	SI	**0.00**	-0.19	-0.40	-0.75	-0.75	-0.40	**0.02**
Brucite	$Mg(OH)_2$	SI	**0.05**	0.17	-0.24	-1.06	-1.16	-0.35	**0.40**
Halite	NaCl	SI	**0.00***	**0.00***	**0.00***	**0.00***	**0.00***	**0.00***	**0.00***
pH			6.9	6.3	5.7	5.2	5.3	5.7	6.9
Cl	Cl^-	mol kg^{-1}	11.6	11.7	11.7	11.9	11.9	11.7	11.6
Mg	Mg^{2+}	mol kg^{-1}	5.59	5.59	5.59	5.59	5.59	5.59	5.59
Na	Na^+	mol kg^{-1}	7.54×10^{-2}	1.20×10^{-1}	1.92×10^{-1}	3.81×10^{-1}	$2.94e\times10^{-1}$	1.92×10^{-1}	7.51×10^{-2}
ΔHalite	Incremental	mol kg^{-1}	0	4.47×10^{-2}	7.19×10^{-2}	1.89×10^{-1}	-8.71×10^{-2}	-1.03×10^{-1}	-1.16×10^{-1}
ΔHalite	Total	mol kg^{-1}	0	4.47×10^{-2}	1.17×10^{-1}	3.06×10^{-1}	2.19×10^{-2}	1.16×10^{-1}	-2.80×10^{-4}

Table 5: A NaCl+$MgCl_2$-brine heat exchange fluid composition and mineral saturation indices (SI) during heating and cooling processes as determined using PHREEQC 3 and Pitzer.dat. Bold numbers indicate saturation or supersaturation, * indicates equilibrium phase.

			Heating (Injection)			Max	Cooling (Extraction)		
Mineral	Formula		10°C	40°C	70°C	120°C	100°C	70°C	10°C
Anhydrite	$CaSO_4$	SI	**0.00**	-0.43	-0.94	-1.91	-1.50	-0.76	**0.01**
Bischofite	$MgCl_2$ * $6H_20$	SI	**0.00**	-0.21	-0.42	-0.76	-0.62	-0.34	**0.01**
Brucite	$Mg(OH)_2$	SI	-0.07	-0.41	-0.83	-1.64	-1.30	-0.69	-0.08
Carnallite	$KMgCl_3$:$6H_2O$	SI	-0.69	-1.44	-2.06	-2.85	-2.56	-1.86	-0.68
Glauberite	$Na_2Ca(SO_4)_2$	SI	-3.49	-4.09	-4.76	-6.06	-5.51	-4.52	-3.49
Goergeyite	$K_2Ca_5(SO_4)6H_2O$	SI	-0.41	-6.38	-11.5	-19.0	-16.1	-9.86	-0.37
Gypsum	$CaSO_4$:$2H_2O$	SI	-0.44	-1.16	-1.90	-3.20	-2.66	-1.64	-0.43
Halite	**NaCl**	**SI**	**0.00***	**0.00***	**0.00***	**0.00***	**0.00***	**0.00***	**0.00***
Kieserite	$MgSO_4$: H_2O	SI	-0.49	-0.94	-1.25	-1.62	-1.48	-1.15	-0.48
Polyhalite	$K_2MgCa_2(SO_4)_4$ * $2H_2O$	SI	-5.42	-8.28	-11.6	-17.9	-15.3	-10.4	-3.5
Sylvite	KCl	SI	-1.84	-2.23	-2.53	-2.92	-2.77	-2.43	-1.43

pH			6.7	5.9	5.4	4.8	5.1	5.6	6.7
Ca	Ca^{2+}	mol kg^{-1}	5.76×10^{-3}	5.76×10^{-3}	5.76×10^{-3}	5.76×10^{-3}	5.76×10^{-3}	5.76×10^{-3}	5.76×10^{-3}
Cl	Cl^{-}	mol kg^{-1}	11.4	11.5	11.6	11.8	11.7	11.6	11.5
Fe	Fe^{3+}	mol kg^{-1}	3.00×10^{-7}	3.00×10^{-7}	3.00×10^{-7}	3.00×10^{-7}	3.00×10^{-7}	3.00×10^{-7}	3.00×10^{-7}
K	K^{+}	mol kg^{-1}	1.93×10^{-3}	1.93×10^{-3}	1.93×10^{-3}	1.93×10^{-3}	1.93×10^{-3}	1.93×10^{-3}	1.93×10^{-3}
Mg	Mg^{2+}	mol kg^{-1}	5.61	5.61	5.61	5.61	5.61	5.61	5.61
Na	Na^{+}	mol kg^{-1}	7.53×10^{-2}	1.20×10^{-1}	1.92×10^{-1}	3.81×10^{-1}	2.94×10^{-1}	1.64×10^{-1}	7.48×10^{-2}
SO_4	SO_4^{2-}	mol kg^{-1}	6.95×10^{-3}	6.95×10^{-3}	6.95×10^{-3}	6.95×10^{-3}	6.95×10^{-3}	6.95×10^{-3}	6.95×10^{-3}
ΔHalite	Incremental	mol L^{-1}	0	4.47×10^{-2}	7.21×10^{-2}	1.89×10^{-1}	-8.75×10^{-2}	-1.30×10^{-1}	-8.92×10^{-2}
ΔHalite	Total	mol L^{-1}	0	4.47×10^{-2}	1.17×10^{-1}	3.06×10^{-1}	2.19×10^{-1}	8.87×10^{-2}	-5.00×10^{-4}

3.2 3-D Reservoir Simulations

A 3-D reactive transport model was used to simulate heat transfer and mass transport in a geothermal doublet system over 30 years. The 3-D reservoir simulation focuses on chemical processes and temperature change within the reservoir (interval 2). A reservoir temperature of 120°C and a reinjection temperature of 70°C were used (Alt-Epping et al., 2013). Hydraulic head at the injection well increases to 34 m head, while head at the production well drops to -16 m, relative to the surface (Figure 4). The pressure at the injection well was 27,551 kPa and at the production well 28,524 kPa. The temperature at the production well is constant at 120°C until it begins to decrease at 7300 days with a decrease by 10950 days of 2.5°C to 117.5°C. Temperatures vary slightly above 120°C due to numerical dispersion that occurs in finite element models.

Two heat exchange fluids were evaluated, NaCl and $MgCl_2$-brines saturated at 10°C. The third bring, $MgCl_2$+NaCl was not evaluated, due to the similarities to the $MgCl_2$-brine. For both heat exchange fluid compositions, the following stages occurred: initially, the formation was saturated with halite at 120°C and a relative pressure of 0 kPa; next, as pumping began, pressure increased near the production well, the temperature decreased, and changes in geochemical composition began; finally, the cool thermal plume and region of geochemical change continued to grow and move toward the production well (Figure 5). The simulations for both the NaCl-brine and $MgCl_2$-brine heat exchange fluids indicate rapid movement of fluid through the formation. Concentration results are presented in mol/L due to the output of the model and complex density changes with temperature and concentration.

Figure 4: A cross-section at the wells of (a) Hydraulic head and (b) temperature in a geothermal doublet system with a pumping rate of 3000 m^3 d^{-1} in the cross-section after 10,950 days (30 years). The fracture density is 1 m^{-1} and fracture aperture is 0.3 mm.

Figure 5: Geothermal doublet aqueous ion concentration after 365 days for a NaCl brine heat exchange fluid, saturated at 10°C (a), and an $MgCl_2$ brine heat exchange fluid, saturated at 10°C (b) injected into a halite formation at 70°C.

The concentrations of Cl^-, Na^+ and Mg^{2+} at the injection and production wells were evaluated (Figure 6). The concentration of Cl^- at the production well begins to decrease, reaching equilibrium at approximately half a year for the NaCl-brine model. This indicates the displacement of the formation water with the injected brine in the flow path (Figure 6). For the $MgCl_2$-brine, Mg^{2+} emerges at the production well, replacing Na^+ and reaching equilibrium after approximately 1 year.

Figure 6: Comparison of Cl^-, Mg^{2+}, and Na^+ concentration at the production well over 730 days (2 years) in a geothermal doublet system initially saturated with NaCl, injected with (a) NaCl-brine and (b) $MgCl_2$-brine heat exchange fluids.

3.2.1 Sensitivity to fracture density (N) and fracture aperture (B)

The pressure, temperature, and geochemical breakthrough indicated sensitivities to fracture aperture and frequency. The difference in head between the injection well and production well was greatest for scenario 5 (Table 2) with tight fractures and infrequent spacing, with a value of 1.35 x10^7 kPa. The lowest pressure, 115 kPa, occurred in scenario 3 with small apertures and frequent fracture spacing. The temperature at the production well began to decrease around 20 years for all simulations except simulation 5, with small, infrequent fractures (Figure 7). Simulations 1, 3, and

4 resulted in similar curves, with an approximate decrease in temperature after 30 years of 2.3°C. Simulation 2 resulted in similar curves with a temperature decrease after 30 years of 1.2°C. Simulation 5 resulted in very little decrease in produced temperature, 0.1°C after 30 years. The breakthrough of Mg^{2+} at the production well was similar for simulations 1, 3, and 4. Breakthroughs for simulations 2 and 5, with high fracture aperture and frequent spacing and lower fracture aperture and infrequent spacing resulting in produced fluids at the production well that were not saturated with Mg^{2+}.

Figure 7: Comparison of sensitivity to fracture frequency (N) and aperture (B) for a) observed temperature at the production well and b) Mg^{2+} at the production well in a geothermal doublet system

Sensitivity to the direction of anisotropy indicated that breakthrough time for temperature decrease is similar for both horizontal flow equal to 10 times vertical flow and the inverse (Figure 8). However, when the flow is increased in the vertical direction (Kz = Ky = 0.1 Kx) temperature at the production well decreases by an additional 3.5°C at 30 years. For the breakthrough of mass, the timing was similar for both directions of anisotropy. However, for Mg^{2+}, the concentration of produced magnesium was reduced by 0.3 mol/L when the flow is increased in the vertical direction.

Figure 8: Comparison of sensitivity to anisotropy for a) observed temperature at the production well and b) Mg^{2+} at the production well in a geothermal doublet system.

4 Discussion

4.1 Chemical Processes within the flow system

4.1.1 Chemical processes within the injection well (interval 1)

Within the injection well, a temperature change from 40°C to 70°C was simulated. This heating increased the solubility of halite, creating the potential for dissolution at the formation. The results indicate that this change in temperature from 40 to 70°C results in potential halite dissolution of 0.239 mol kg^{-1} for the NaCl-brine, 0.072 mol L^{-1} for the $MgCl_2$-brine and 0.072 mol L^{-1} for the NaCl+$MgCl_2$-brine. The initial saturated composition of the heat exchange fluids was at 10°C. The results indicate that this change in temperature from 10 to 70°C results in potential halite dissolution of 0.350 mol L^{-1} for the NaCl-brine, 0.117 mol L^{-1} for the $MgCl_2$-brine and 0.117 mol L^{-1} for the NaCl+$MgCl_2$-brine. This indicates that the smallest halite dissolution potential is created when using the $MgCl_2$ and NaCl+$MgCl_2$-brines. These findings agree with Nishri et al. (1988) who described that the solubility of halite decreases in the presence of dissolved $MgCl_2$.

The high ionic composition and changes in temperature and pressure also create the potential for additional mineral precipitation. Minimal precipitation is expected within the injection well, as temperature and pressure are increasing, which both generally increase the solubility of halite. The $MgCl_2$-brine results indicate the potential for brucite and anhydrite mineral precipitation within the injection well. The brucite precipitation can generally be controlled using phosphonic acid (Scheiber et al., 2014).

4.1.2 Chemical processes within the reservoir (interval 2)

The processes within the reservoir were simulated in both the batch reaction model and 3-D model. Within the reservoir the greatest amount of fluid heating occurred, as temperature increased from 70°C to 120°C. The pressure within the reservoir was highest at the injection well and lowest at the production well. Temperature is the primary driver of the fluid solubility, with

the fluid entering the formation undersaturated with halite. However, for halite, high pressure increases solubility, and low pressure decreases solubility.

Considering temperature in the batch reaction simulation, the estimated halite dissolution is greatest using the NaCl-brine, 0.829 mol kg^{-1}, then $MgCl_2$-brine, 0.306 mol kg^{-1} and NaCl+$MgCl_2$-brine, 0.306 mol kg^{-1}. During the simulation of the saturated $MgCl_2$–brine in the halite formation, the region near the injection well was saturated with Cl^- and Mg^{2+}, while Na^+ decreased as a result of the common ion effect (Figure 6). The $MgCl_2$ and NaCl+$MgCl_2$-brines resulted in increased preservation of the halite formation.

In the 3-D, 30-year simulation, the concentration and temperature gradients for the inflowing temperature and heat exchange fluid were generally sharp (Figure 4, Figure 5). The 3-D model indicates that the injected fluid moved quickly through the formation, with the produced fluid constant after approximately 365 days. However, depending on the permeability and porosity of the formation, and the fracture or matrix properties, this may occur earlier (Figure 7).

Dissolution is most likely to occur at the front of the temperature plume, and progress over time with the front. The progression of a fluid through halite as a front versus channelized flow depends on the flow rate (Weisbrod et al., 2012). Borgia et al. (2012) observed an advancing front of NaCl that moved from the injection well to the production well similar to what we expect based on the temperature profile. Dissolution is expected to occur at the temperature front, whereas precipitation is expected to occur near the production well and when the fluid begins to cool, as it moves up through the geothermal well (Bächler and Kohl, 2005; Borgia et al., 2012). Weisbrod et al. (2012) found that flow rates control whether brines move as a propagating front or through channels, and at low flow rates, salt precipitation resulting in clogging was more likely to occur.

4.1.3 Chemical processes within the production well (interval 3)

As the fluid moves up the production well, it begins at maximum temperature, 120°C, and cools to an estimated 100°C. This cooling process results in precipitation of halite. This change in temperature results in a 0.196 mol kg^{-1} precipitation of halite for the NaCl-brine, 0.087 mol kg^{-1} for the $MgCl_2$-brine, and 0.088 mol kg^{-1} for the NaCl+$MgCl_2$-brine. This indicates that the $MgCl_2$-brine will result in the least amount of precipitation in the production well. Pressure changes from 0.1 to 30 MPa can be used to increase or decrease the solubility of halite and NaCl solutions by 0.045 mol kg^{-1}, however smaller changes in solubility are observed in the $MgCl_2$ and NaCl+$MgCl_2$-brines, at 0.0017 mol kg^{-1}.

Decreasing pressure at the production well in the reservoir results in decreased solubility for high-temperature solutions. Increasing pressure in the production well at the surface results in increased solubility when temperatures are cooling. Therefore, although the NaCl-brine has a larger solubility change with temperature, it is easier to control with pressure.

4.1.4 Chemical processes within the surface production (interval 4)

Within the surface production, a change in temperature from 100°C to 70°C is expected. The results indicate that this change in temperature results in a 0.282 mol kg^{-1} for the NaCl-brine, 0.189 mol kg^{-1} for the $MgCl_2$-brine, and 0.130 mol kg^{-1} for the NaCl+$MgCl_2$-brine. This indicates that the NaCl+$MgCl_2$-brine will result in the least amount of precipitation at the surface. Halite precipitation at the surface could be collected as a mining process; however additional study is required to determine the effect this would have on the permeability and flow within the formation.

The consideration of the brine cooling to 10°C was also evaluated. The change from 120°C to 10°C results in a 0.83 mol kg^{-1} for the NaCl-brine, 0.306 mol kg^{-1} for the $MgCl_2$-brine, and 0.305 mol kg^{-1} for the NaCl+$MgCl_2$-brine.

4.2 Implications of a modified heat exchange fluid

Chemical inhibitors are used to reduce scaling in geothermal and oil and gas wells, e.g. Alt-Epping et al. (2013) The concept of designing a heat exchange fluid is similar to the use of inhibitors. Trace metals and aqueous trace ions, I^-, Br^- and F^- are considered to inhibit halite dissolution (Alkattan et al., 1997a, b). In oil and gas, halite is considered difficult to control and is treated with freshwater flushes (Chen et al., 2009). Wellbore cleanout and mechanical tools have also been used in halite clogged wells; however, the effects were short-lived (Soomro et al., 2015). However, controlling optimum pressure at depth for the given fluid chemistry was found to decrease salt precipitation in the well (Soomro et al., 2015). Therefore, a combination of a designed heat exchange fluid with pressure control may be an effective method for reducing precipitation or controlling the composition of precipitates.

At the maximum expected flow rate in such a system, of 6000 m^3 d^{-1}, and a concentration of 5.61 mol L^{-1} Mg^{2+}, the process would require 3210 tonnes d^{-1} of $MgCl_2$. Much of this could be recycled after the first year. The NaCl-brine results in 70 tonnes d^{-1} NaCl produced, the $MgCl_2$-brine 32 tonnes d^{-1} NaCl and the NaCl+$MgCl_2$-brine 31 tonnes day^{-1} NaCl. In comparison, American Rock Salt Co., which operates the largest salt mine in the United States produces approximately 9000 to 16000 tonnes d^{-1} (American Rock Salt, 2019). Continuous mining of the formation would result in a large cavity, producing the potential for increased flow through the formation or collapse and potential sinkhole formation, e.g. Johnson (1989).

4.3 Limitations and Future Work

This model works under the assumption that the porosity and permeability will remain relatively consistent with time. The matrix was assumed to be nondeforming with constant porosity and permeability throughout the simulations. However, within the Williston Basin Devonian salts, brittle behaviour, and plastic salt creep have been observed (Scott Duncan and Lajtai, 1993). Deformation, therefore, can result in both the closing and opening of fractures simultaneously. Open and closing of fractures is also controlled by dissolution and precipitation (Blaisonneau et al., 2016). Creep in a geothermal system, unlike creep in an open cavity, can be prevented by maintaining fluid pressure to balance stresses and strains (Warren, 2006). However, this may be difficult during shut down in production. The physical opening and closing of porosity and permeability due to deformation, salt creep, and dissolution and precipitation warrants further study.

The batch reaction analysis was limited by the simplified geometry. However, it provides excellent insight into the complex chemical reactions that occur as the heat exchange fluid changes temperature. The results would benefit from calibration field data; however, such data do not exist.

The 3-D simulations were limited by the assumption that the fractures expected in the system can be simulated using a matrix. A matrix has been shown to accurately simulate a fractured reservoir when calibrated (Blessent et al., 2014; Jain et al., 2015; Jarrahi et al., 2019). However, without calibration data, the simulation is more uncertain. Some numerical instability was observed in the simulations. Negative concentration values occur in finite elements solutions near sharp concentration fronts due to oscillatory behavior (Wissmeier, 2015). Negative concentrations are set to zero during reaction calculations, then added to the output concentrations from the reaction step (Wissmeier, 2015). In this way, mass balance errors are remedied.

5 Conclusions

Halite formations have high thermal conductivity, which can result in substantial thermal anomalies at the top of the formations. Low temperature geothermal systems for power production can benefit from such thermal anomalies. This study characterizes the complex geochemistry associated with halite to inform decisions to develop such a system. This included calculating the quantities of dissolved or precipitated minerals throughout major changes in pressure and temperature in the system and characterizing the potential dissolution inhibition using $MgCl_2$ in the injected heat exchange fluid.

Numerical simulations were used to characterize heat exchange fluids in a highly saline binary geothermal system. The numerical simulations were beneficial in understanding the complex precipitation and dissolution that occur within geothermal systems targeting halite formations with changes to pressure and temperature. A NaCl-brine, $MgCl_2$-brine, and NaCl+$MgCl_2$-brine, each saturated at 10°C, were characterized in the Prairie Evaporite, a formation dominated by halite. The 3-D simulation used a 618 m well spacing, 6000 m^3 d^{-1} flow rate, and an equivalent porous media were used to represent the fractured area. Temperatures ranged from 70 to 120°C.

The batch reaction simulations indicated the brines containing $MgCl_2$ reduced dissolution within the halite formation compared to the NaCl-brine. The pure $MgCl_2$-brine resulted in the smallest amount of dissolution in the formation, with 0.195 mol kg^{-1} less dissolution in the formation than the NaCl-brine. The NaCl+$MgCl_2$-brine resulted in the least precipitation in the production well, with 0.152 mol kg^{-1} less precipitation in the production well compared to the NaCl-brine. This indicates that $MgCl_2$ can be used as an inhibitor to precipitation and dissolution in a halite reservoir. When comparing solubility under pressure, the NaCl-brine was susceptible to

changes in pressure, with up to a 0.045 mol kg^{-1} change in solubility between 0.1 and 30 MPa. The $MgCl_2$ and NaCl+$MgCl_2$-brines produced only a 0.0017 mol kg^{-1} change in solubility over the same pressure change. By carefully controlling temperature and pressure within the production well, risks of clogging can be reduced.

The $MgCl_2$-brine works to reduce precipitation within the formation. Based on 3-D simulations, the emergence of the $MgCl_2$-brine at the production well increased to steady-state by 365 days. Therefore, Mg^{2+} could potentially be recycled throughout the lifetime of the well.

Further study into wells in halite systems would benefit from field observations to provide calibration data for model data. Geochemical modeling is an important tool in the development of geothermal systems, providing an understanding of the processes that result in well clogging and potential inhibitors.

Declarations

No declarations.

Availability of data and materials

The numerical simulation data used to support the findings of this study are included in the article.

Competing Interests

The authors declare that there is no competing interest regarding the publication of this paper.

Funding

This work was supported by the Natural Sciences and Engineering Research Council of Canada Vanier Canada Graduate Scholarship program and the Manitoba Graduate Scholarship Program.

Authors' contributions

KM: Project conceptualization, methodology development, data acquisition, modeling simulations, original draft, and editing. HH Project conceptualization, criticized methodology, supervision, review and editing. Both authors read and approved the final manuscript.

Acknowledgements

The authors would like to thank John Christie at ERCO Worldwide for providing the geochemical data from the Prairie Evaporite. We acknowledge review comments from Dr. Allan Woodbury, Dr. Jörg Stetefeld, and Dr. Beata Gorczyca. Finally, thanks to the anonymous reviewers of this paper.

References

Alkattan, M.; Oelkers, E.H.; Dandurand, J.-L.; Schott, J. Experimental studies of halite dissolution kinetics, I The effect of saturation state and the presence of trace metals. Chem Geol. 1997a;137(3–4):201-219.

Alkattan, M.; Oelkers, E.H.; Dandurand, J.-L.; Schott, J. Experimental studies of halite dissolution kinetics: II. The effect of the presence of aqueous trace anions and K3Fe(CN)6. Chem Geol. 1997b;143(1–2):17-26.

Alt-Epping, P.; Waber, H.N.; Diamond, L.W.; Eichinger, L. Reactive transport modeling of the geothermal system at Bad Blumau, Austria: Implications of the combined extraction of heat and CO2. Geothermics. 2013;45:18-30.

American Rock Salt. American Rock Salt: About Us; [cited 2019 4 January 2019]. Available from: https://www.americanrocksalt.com/aboutus

Appelo, C.A.J.; Postma, D. Geochemistry, groundwater and pollution. 2 ed. Amsterdam: A.A. Balkema Publishers; 2005. 649 p.

Axelsson, G.; Gunnlaugsson, E. Long-term monitoring of high- and low-enthalpy fields under exploitation., World Geothermal Congress 2000 Short Course. Kokonoe, Japan: International Geothermal Association; 2000. p. 226.

Bächler, D.; Kohl, T. Coupled thermal–hydraulic–chemical modelling of enhanced geothermal systems. Geophysical Journal International. 2005;161(2):533-548.

Beauheim, R.L.; Domski, P.S.; Roberts, R.M. Hydraulic Testing of Salado Formation Evaporites at the Waste Isolation Pilot Plant Site: Final Report. Sandia National Labs., Albuquerque, NM (US); Sandia National Labs., Livermore, CA (US); 1999.

Bezys, R.K.; McCabe, H.R. Lower to middle Paleozoic stratigraphy of southwestern Manitoba. Winnipeg, Manitoba: Geological Association of Canada; 1996.

Blaisonneau, A.; Peter-Borie, M.; Gentier, S. Evolution of fracture permeability with respect to fluid/rock interactions under thermohydromechanical conditions: development of experimental reactive percolation tests. Geothermal Energy. 2016;4(1):3.

Blessent, D.; Jørgensen, P.R.; Therrien, R. Comparing Discrete Fracture and Continuum Models to Predict Contaminant Transport in Fractured Porous Media. Groundwater. 2014;52(1):84-95.

Borgia, A.; Pruess, K.; Kneafsey, T.J.; Oldenburg, C.M.; Pan, L. Numerical simulation of salt precipitation in the fractures of a CO2-enhanced geothermal system. Geothermics. 2012;44:13-22.

Bujakowski, W.; Barbacki, A.; Miecznik, M.; Pająk, L.; Skrzypczak, R.; Sowiżdżał, A. Modelling geothermal and operating parameters of EGS installations in the lower triassic sedimentary formations of the central Poland area. Renewable Energy. 2015;80(0):441-453.

Chen, T.; Montgomerie, H.; Chen, P.; Vikane, O.; Jackson, T. Understanding the Mechanisms of Halite Inhibition and Evaluation of Halite Scale Inhibitor by Static and Dynamic Tests. SPE International Symposium on Oilfield Chemistry. The Woodlands. Texas: Society of Petroleum Engineers; 2009. p. 8.

Christie, J. To: Moore, K. 2015. Personal Communication.

Daniilidis, A.; Herber, R. Salt intrusions providing a new geothermal exploration target for higher energy recovery at shallower depths. Energy. 2017;118:658-670.

Dehkordi, S.E.; Schincariol, R.A.; Olofsson, B. Impact of Groundwater Flow and Energy Load on Multiple Borehole Heat Exchangers. Groundwater. 2014:n/a-n/a.

Diersch, H. FEFLOW Finite Element Modeling of Flow, Mass and Heat Transport in Porous and Fractured Media. New York: Springer; 2014.

DiPippo, R. Second Law assessment of binary plants generating power from low-temperature geothermal fluids. Geothermics. 2004;33(5):565-586.
Earl, S.L.; Nahm, J.J. Use Of Chemical Salt Precipitation Inhibitors To Maintain Supersaturated Salt Muds For Drilling Salt Formations. Society of Petroleum Engineers; 1981.
Ferguson, G.; Grasby, S. The geothermal potential of the basal clastics of Saskatchewan, Canada. Hydrogeol J. 2014;22(1):143-150.
Firoozy, N. Assessment of Geothermal Application for Electricity Production from the Prairie Evaporite Formation of Williston Basin in South-West Manitoba [Winnipeg, Manitoba]: University of Manitoba; 2016. 165 p.
Fisher, M.K.; Warpinski, N.R. Hydraulic-fracture-height growth: Real data. SPE Production & Operations. 2012;27(01):8-19.
Frick, S.; Regenspurg, S.; Kranz, S.; Milsch, H.; Saadat, A.; Francke, H.; Brandt, W.; Huenges, E. Geochemical and Process Engineering Challenges for Geothermal Power Generation. Chemie Ingenieur Technik. 2011;83(12):2093-2104.
Fu, Y.; van Berk, W.; Schulz, H.-M. Hydrogeochemical modelling of fluid–rock interactions triggered by seawater injection into oil reservoirs: Case study Miller field (UK North Sea). Appl Geochem. 2012;27(6):1266-1277.
Garven, G. Continental-Scale Groundwater Flow and Geologic Processes. Annual Review of Earth and Planetary Sciences. 1995;23(1):89-117.
Grasby, S.E.; Allen, D.M.; Bell, S.; Chen, Z.; Ferguson, G.; Jessop, A.; Kelman, M.; Ko, M.; Majorowicz, J.; Moore, M.; Raymond, J.; Therrien, R. Geothermal Energy Resource Potential of Canada. Calgary, AB: Geological Survey of Canada; 2012.
Grobe, M. Distribution and thickness of salt within the Devonian Elk Point Group, Western Canada Sedimentary Basin. Edmonton, Alberta: Alberta Energy and Utilities Board; 2000.
Gunnlaugsson, E.; Ármannsson, H.; Thorhallsson, S.; Steingrímsson, B. Problems in geothermal operation-scaling and corrosion. In: UNU_GTP; LaGeo, editors, Short Course VI on Utilization of Low- and Medium-Enthalpy Geothermal Resources and Financial Aspects of Utilization. Santa Tecla, El Salvador; 2014.
Hadgu, T.; Kalinina, E.; Lowry, T.S. Modeling of heat extraction from variably fractured porous media in Enhanced Geothermal Systems. Geothermics. 2016;61:75-85.
Hesshaus, A.; Houben, G.; Kringel, R. Halite clogging in a deep geothermal well – Geochemical and isotopic characterisation of salt origin. Physics and Chemistry of the Earth, Parts A/B/C. 2013;64(0):127-139.
Jacek, M.; Stephen, E.G. Heat flow, depth–temperature variations and stored thermal energy for enhanced geothermal systems in Canada. Journal of Geophysics and Engineering. 2010;7(3):232.
Jain, C.; Vogt, C.; Clauser, C. Maximum Potential for Geothermal Power in Germany Based on Engineered Geothermal Systems. Geothermal Energy. 2015;3(15):1-20.
Jarrahi, M.; Moore, K.R.; Holländer, H.M. Comparison of solute/heat transport in fractured formations using discrete fracture and equivalent porous media modeling at the reservoir scale. Physics and Chemistry of the Earth, Parts A/B/C. 2019.
Johnson, K.S. Development of the Wink Sink in west Texas, U.S.A., due to salt dissolution and collapse. Environmental Geology and Water Sciences. 1989;14(2):81-92.
Kalinina, E.A.; Klise, K.A.; McKenna, S.A.; Hadgu, T.; Lowry, T.S. Applications of fractured continuum model to enhanced geothermal system heat extraction problems. Springerplus. 2014;3:110-110.

Lach, A.; Ballerat-Busserolles, K.; André, L.; Simond, M.; Lassin, A.; Cézac, P.; Neyt, J.-C.; Serin, J.-P. Experimental Data and Modeling of Solution Density and Heat Capacity in the Na–K–Ca–Mg–Cl–H2O System up to 353.15 K and 5 mol·kg–1 Ionic Strength. Journal of Chemical & Engineering Data. 2017;62(10):3561-3576.
Ledésert, B.A.; Hébert, R.L. The Soultz-sous-Forêts' Enhanced Geothermal System: A Granitic Basement Used as a Heat Exchanger to Produce Electricity. In: Mitrovic, J., editor, Heat Exchangers - Basic Design Applications: INTECH Open Access Publisher; 2012. p. 477 - 504.
Legarth, B.; Huenges, E.; Zimmermann, G. Hydraulic fracturing in a sedimentary geothermal reservoir: Results and implications. Int J Rock Mech Min. 2005;42(7–8):1028-1041.
Limberger, J.; Boxem, T.; Pluymaekers, M.; Bruhn, D.; Manzella, A.; Calcagno, P.; Beekman, F.; Cloetingh, S.; van Wees, J.-D. Geothermal energy in deep aquifers: A global assessment of the resource base for direct heat utilization. Renewable and Sustainable Energy Reviews. 2018;82:961-975.
Luo, F.; Xu, R.-N.; Jiang, P.-X. Numerical investigation of fluid flow and heat transfer in a doublet enhanced geothermal system with CO2 as the working fluid (CO2–EGS). Energy. 2014;64:307-322.
Majorowicz, J.; Grasby, S.E. Heat flow, depth–temperature variations and stored thermal energy for enhanced geothermal systems in Canada. Journal of Geophysics and Engineering. 2010;7(3):232.
Majorowicz, J.; Moore, M. The feasibility and potential of geothermal heat in the deep Alberta foreland basin-Canada for CO2 savings. Renewable Energy. 2014;66(0):541-549.
Manz, L.A., cartographer. Deep Geothermal Resources: Estimated Temperatures on Top of the Duperow Formation Kenmare 100K Sheet, North Dakota [map]. Bismark, ND: North Dakota Geological Survey; 2011. (North Dakota Geothermal Maps).
Moore, K.R.; Holländer, H.M. Geochemical Modelling of the Dissolution of Salt Minerals and Application to Geothermal Energy. GeoOttawa 2017. Ottawa, Canada: Canadian Geotechnical Society; 2017.
Moore, K.R.; Holländer, H.M. Feasibility of low-temperature geothermal systems: Considerations of thermal anomalies, geochemistry, and local assets. Applied Energy. 2020;275:115412.
Nalla, G.; Shook, G.M.; Mines, G.L.; Bloomfield, K.K. Parametric sensitivity study of operating and design variables in wellbore heat exchangers. Geothermics. 2005;34(3):330-346.
Nishri, A.; Herbert, H.J.; Jockwer, N.; Stichler, W. The geochemistry of brines and minerals from the Asse Salt Mine, Germany. Appl Geochem. 1988;3(3):317-332.
Ozbek, H.; Fair, J.; Phillips, S. Viscosity of Aqueous Sodium Chloride Solutions From 0-150°C. Berkeley, CA: Lawrence Berkeley National Lab; 1977.
Parkhurst, D.L.; Appelo, C. Description of input and examples for PHREEQC version 3--A computer program for speciation, batch-reaction, one-dimensional transport, and inverse geochemical calculations. In: Survey, U.S.G., editor, US Geological Survey Techniques and Methods Section A, Groundwater Book 6, Modeling Techniques. Denver, Colorado; 2013. p. 497.
Petersen, K.; Lerche, I. Quantification of thermal anomalies in sediments around salt structures. Geothermics. 1995;24(2):253-268.
Plummer, L.N.; Parkhurst, D.L.; Fleming, G.W.; Dunkle, S.A. A computer program incorporating pitzer's equations for calculation of geochemical reactions in brines. In: Interior, U.S.D.o.t.; Survey, U.S.G., editors. Reston, Virginia; 1988. p. 310.
Plummer, M.A.; Xia, Y.; Podgorney, R.; Mattson, E.; Huang, H.; Ghassemi, A. Primary Constraints on the Design of an Enhanced Geothermal System Reservoir. 50th US Rock

Mechanics/Geomechanics Symposium. Houston, Texas: American Rock Mechanics Association; 2016. p. 12.
Scheck-Wenderoth, M.; Cacace, M.; Maystrenko, Y.P.; Cherubini, Y.; Noack, V.; Kaiser, B.O.; Sippel, J.; Björn, L. Models of heat transport in the Central European Basin System: Effective mechanisms at different scales. Mar Petrol Geol. 2014;55:315-331.
Scheiber, J.; Seibt, A.; Birner, J.; Cuenot, N.; Genter, A.; Moeckes, W. Barite scale control at the Soultz-sous-Forêts (France) EGS site. Proceedings Thirty-Eighth Workshop on Geothermal Reservoir Engineering. Stanford, California; 2014.
Scott Duncan, E.J.; Lajtai, E.Z. The creep of potash salt rocks from Saskatchewan. Geotechnical & Geological Engineering. 1993;11(3):159-184.
Snow, D.T. Rock fracture spacings, openings, and porosities. Proceedings of the American Society of Civil Engineers. 1968;94:73-91.
Soomro, A.A.; Hadi, A.; Awase, A.; Koondhar, N.H.; Ahmed, N. Method To Optimally Produce Wells Having Salt Precipitation Issues. SPE/PAPG Pakistan section Annual Technical Conference. Islamabad, Pakistan: Society of Petroleum Engineers; 2015. p. 7.
TGI Williston Basin Working Group, cartographer. Devonian Prairie Evaporite: structure contour [map]. Winnipeg, MB; 2008: 1:1000000. (Stratigraphic Map SM2008-DPE-S).
Todaka, N.; Akasaka, C.; Xu, T.; Pruess, K. Reactive geothermal transport simulations to study the formation mechanism of an impermeable barrier between acidic and neutral fluid zones in the Onikobe Geothermal Field, Japan. Journal of Geophysical Research: Solid Earth. 2004;109(B5).
Walsh, W. Geothermal resource assessment of the Clarke Lake Gas Field, Fort Nelson, British Columbia. Bulletin of Canadian petroleum geology. 2013;61(3):241-251.
Wanner, C.; Peiffer, L.; Sonnenthal, E.; Spycher, N.; Iovenitti, J.; Kennedy, B.M. Reactive transport modeling of the Dixie Valley geothermal area: Insights on flow and geothermometry. Geothermics. 2014;51:130-141.
Warren, J.K. Evaporites: sediments, resources and hydrocarbons: Springer Science & Business Media; 2006.
Weisbrod, N.; Alon-Mordish, C.; Konen, E.; Yechieli, Y. Dynamic dissolution of halite rock during flow of diluted saline solutions. Geophysical Research Letters. 2012;39(9).
Winkler, M. Generation-4 Integrated Reservoir Modeling Report. 2011.
Wissmeier, L. piChem - A FELOW Plugin for Advanced Geochemical Reactions. Version 1. Hørsholm, Denmark; 2015. 28.
Xia, Y.; Plummer, M.; Mattson, E.; Podgorney, R.; Ghassemi, A. Design, modeling, and evaluation of a doublet heat extraction model in enhanced geothermal systems. Renewable Energy. 2017;105:232-247.

Figures

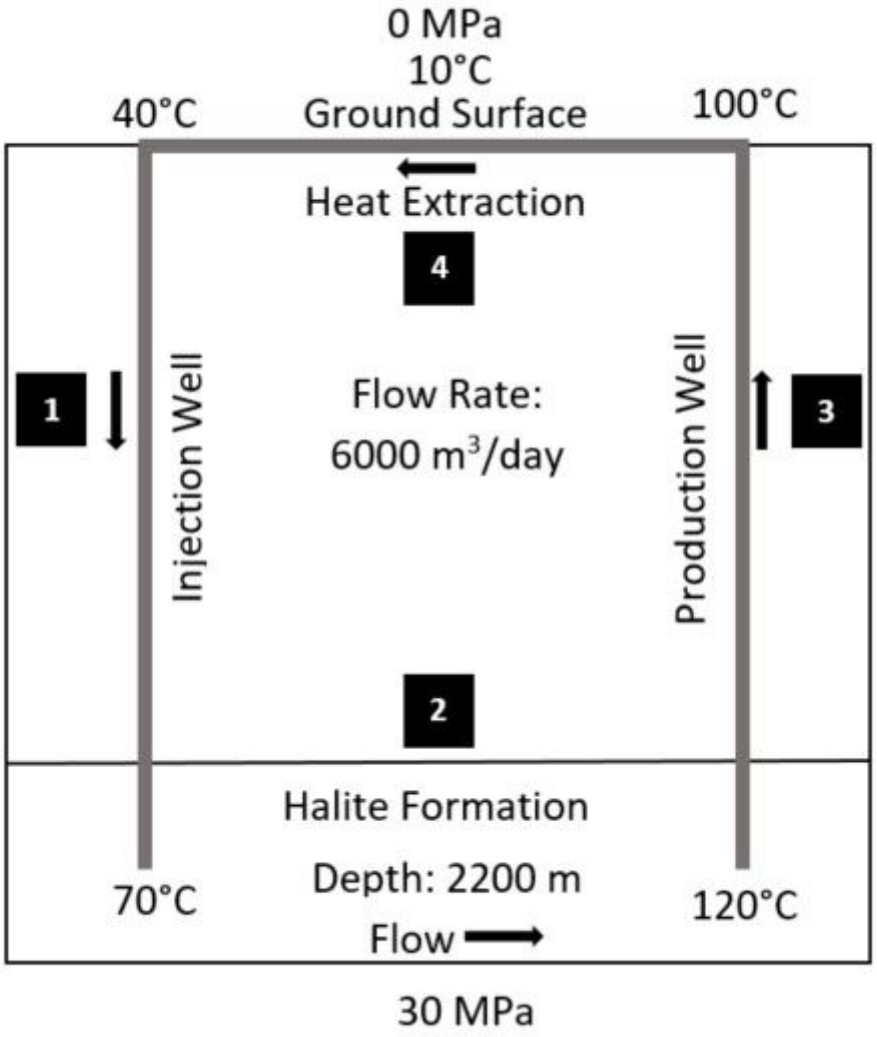

Figure 1

Conceptual model with injection well, halite reservoir, production well, and surface conditions. Shown are the temperature conditions and flow rates. Also shown are the 4 intervals discussed in 2.3.1.

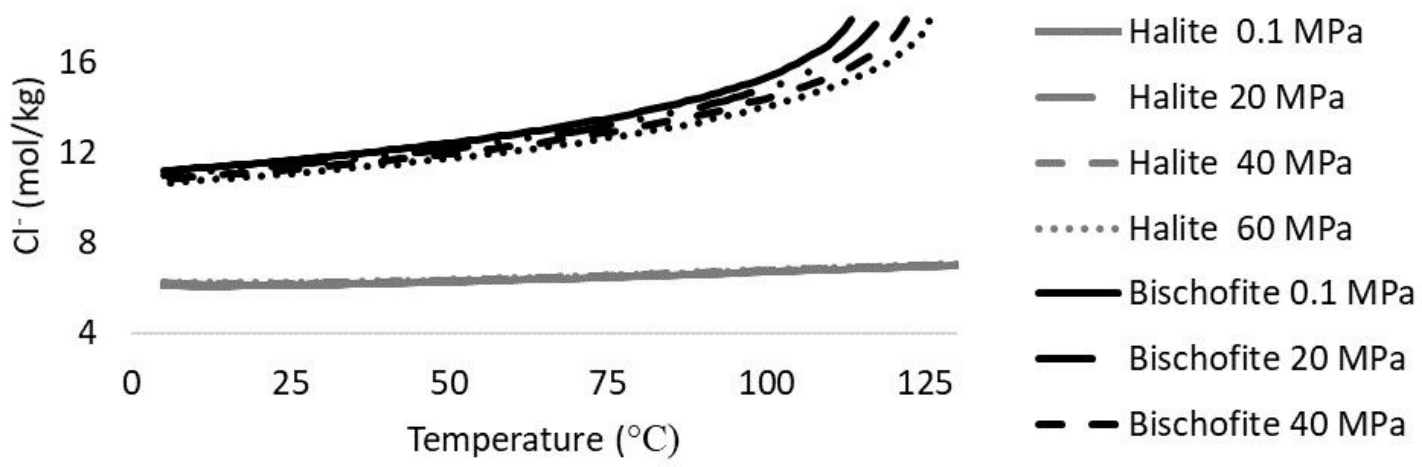

Figure 2

Cl- concentration in solution for halite and bischofite solutions in freshwater with changes in temperature and pressure from the Pitzer.dat from Moore and Holländer (2017)

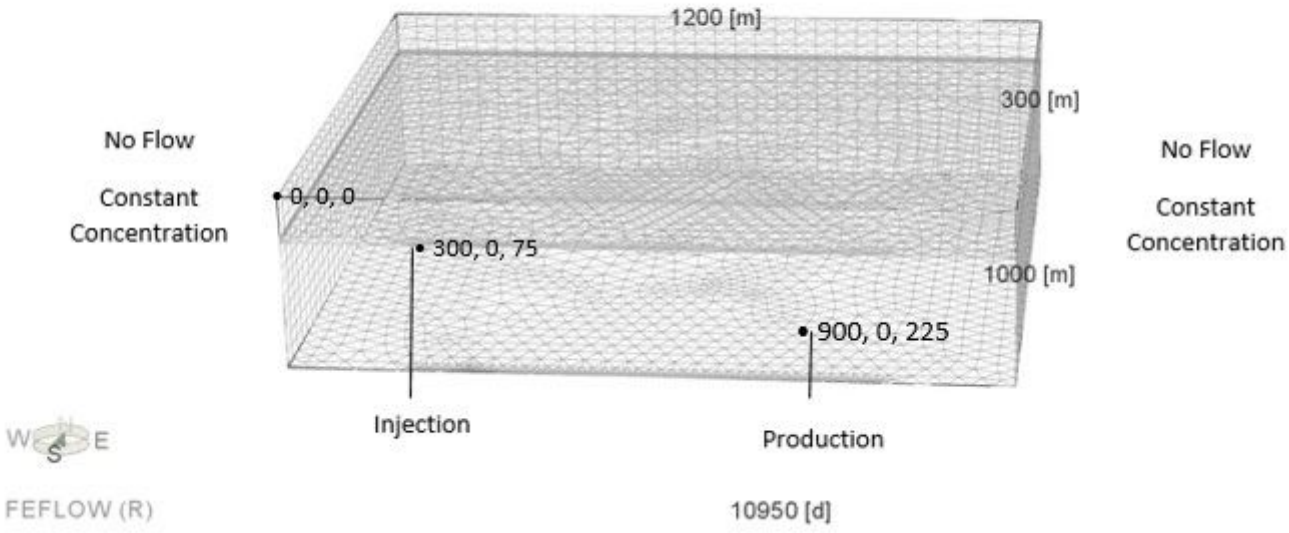

Figure 3

3-D model domain and boundaries for a binary geothermal doublet.

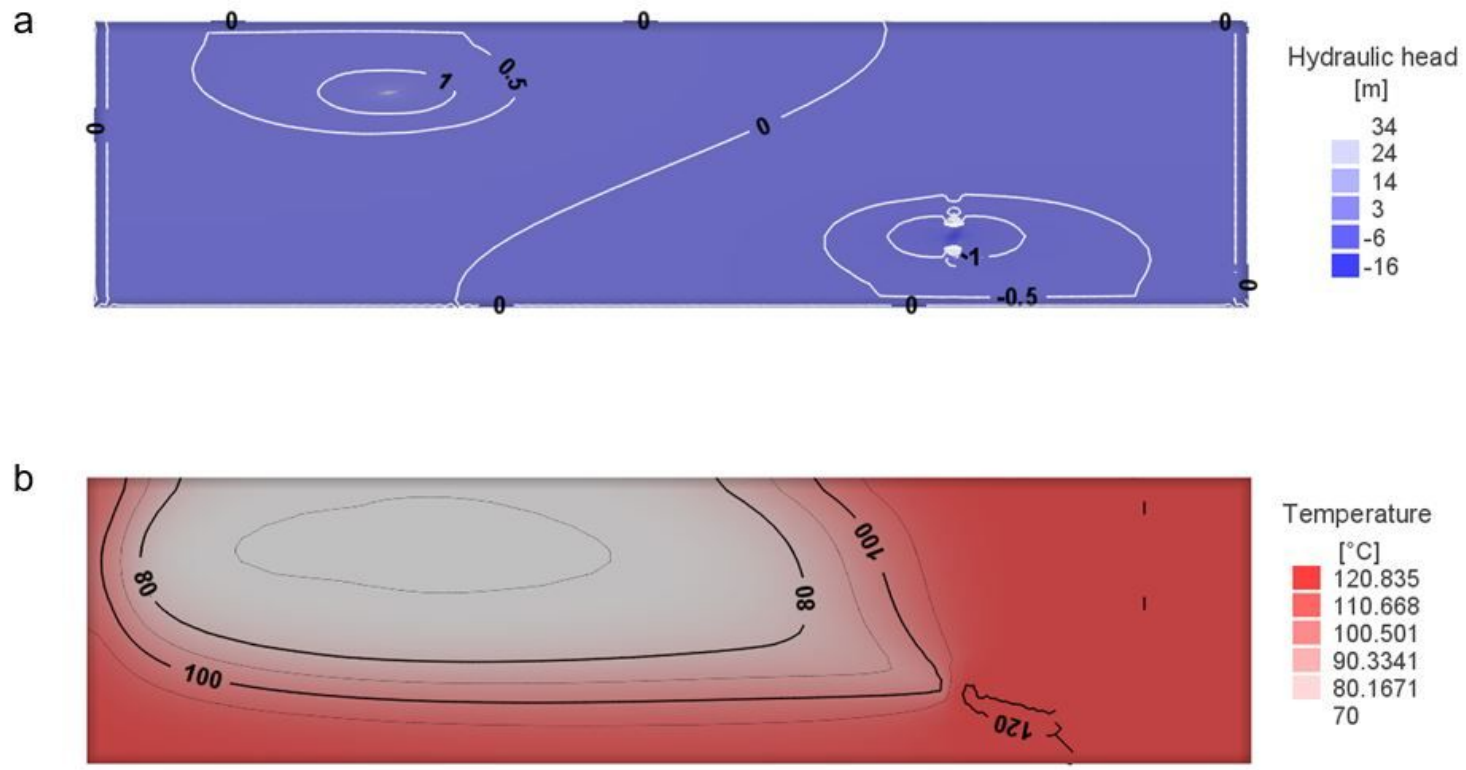

Figure 4

A cross-section at the wells of (a) Hydraulic head and (b) temperature in a geothermal doublet system with a pumping rate of 3000 m3 d-1 in the cross-section after 10,950 days (30 years). The fracture density is 1 m-1 and fracture aperture is 0.3 mm.

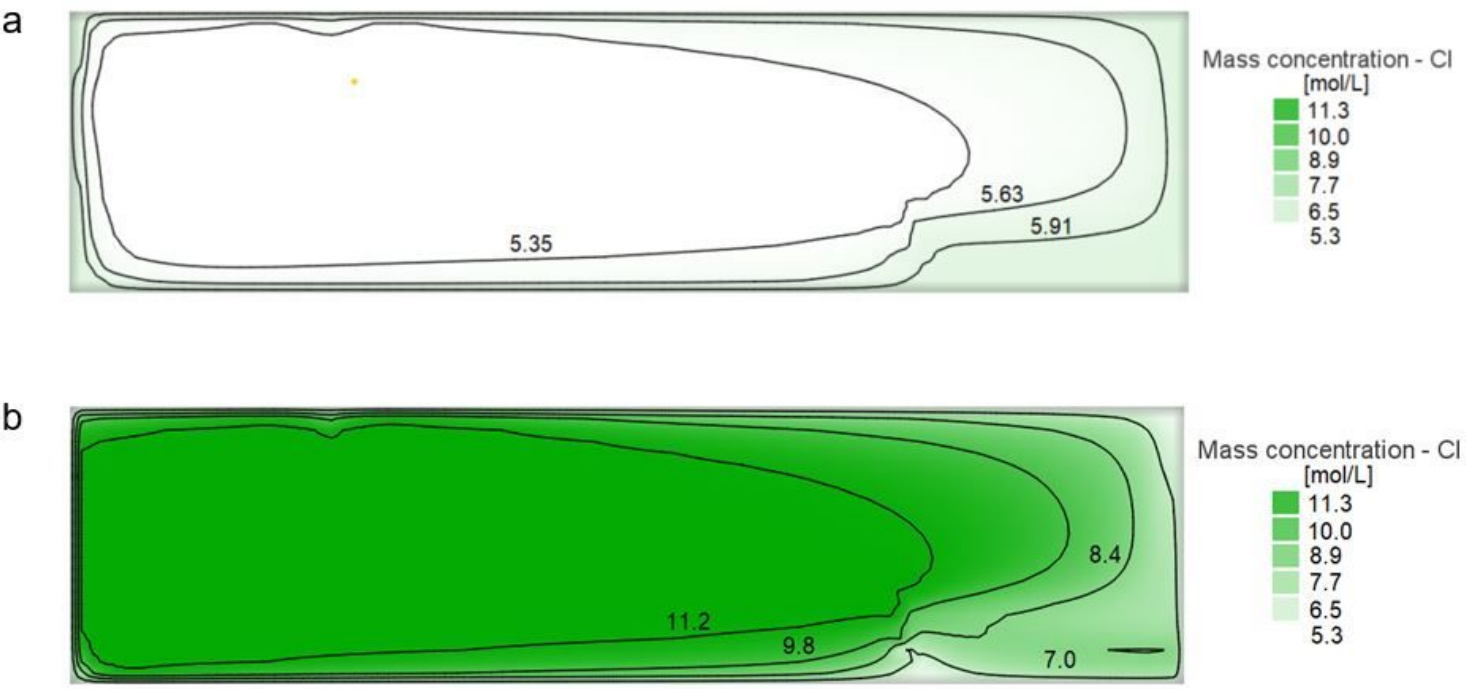

Figure 5

Geothermal doublet aqueous ion concentration after 365 days for a NaCl brine heat exchange fluid, saturated at 10°C (a), and an MgCl2 brine heat exchange fluid, saturated at 10°C (b) injected into a halite formation at 70°C.

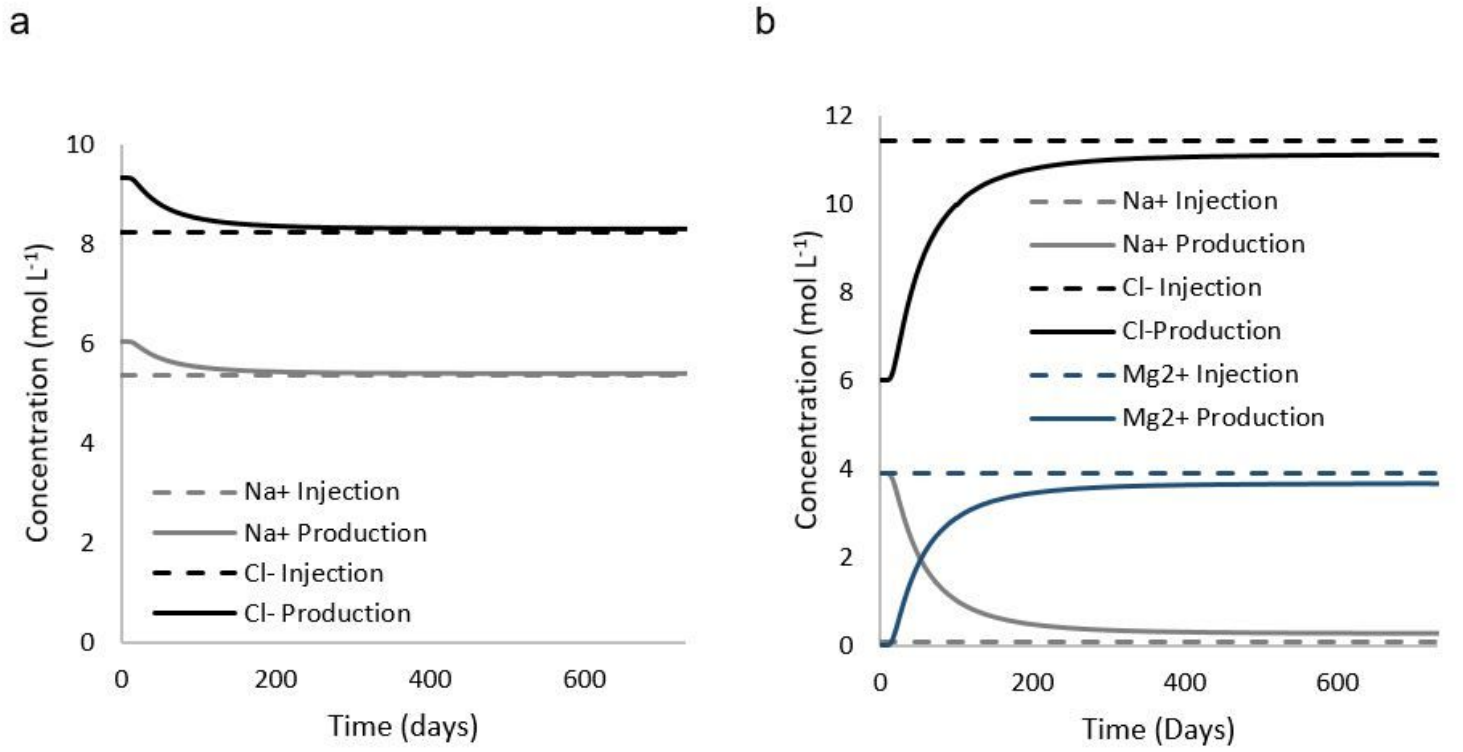

Figure 6

Comparison of Cl-, Mg2+, and Na+ concentration at the production well over 730 days (2 years) in a geothermal doublet system initially saturated with NaCl, injected with (a) NaCl-brine and (b) MgCl2-brine heat exchange fluids.

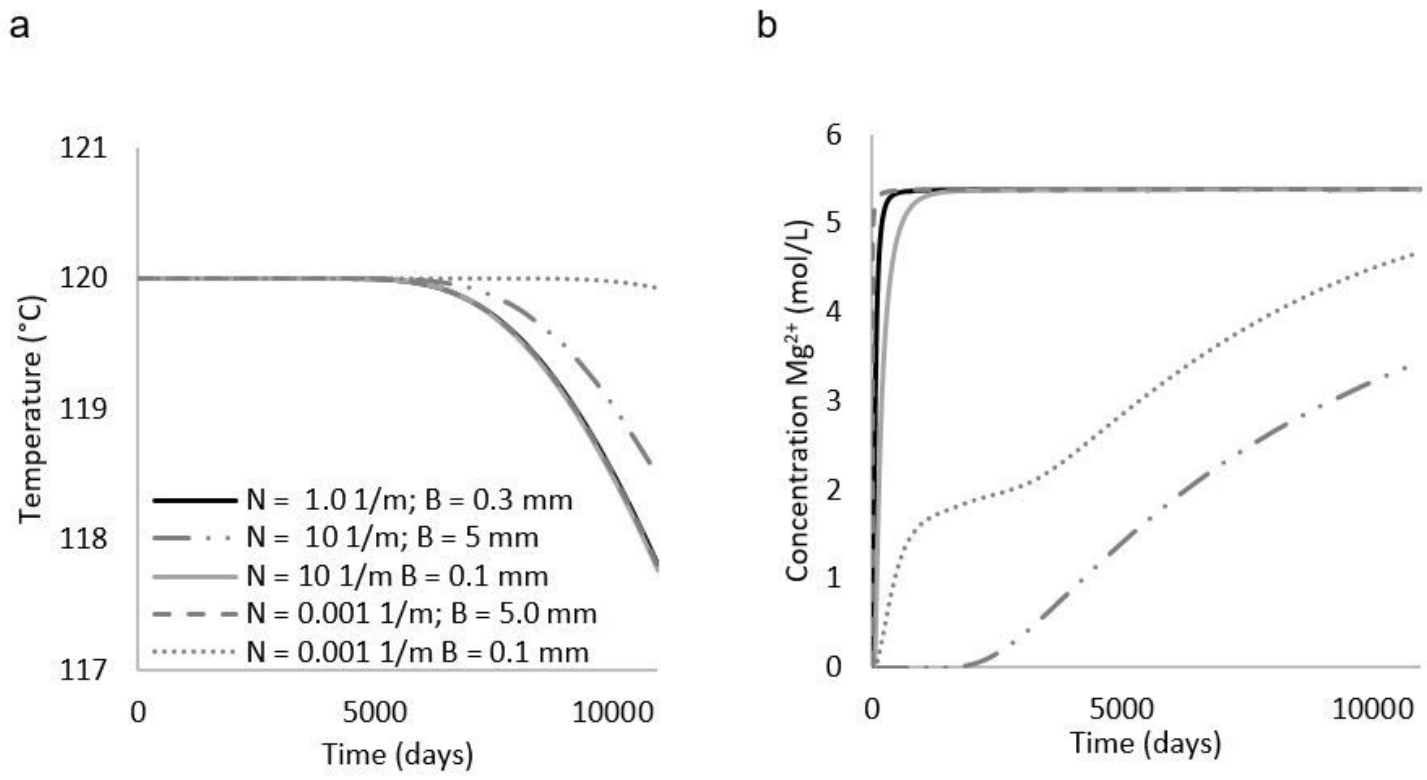

Figure 7

Comparison of sensitivity to fracture frequency (N) and aperture (B) for a) observed temperature at the production well and b) Mg2+ at the production well in a geothermal doublet system

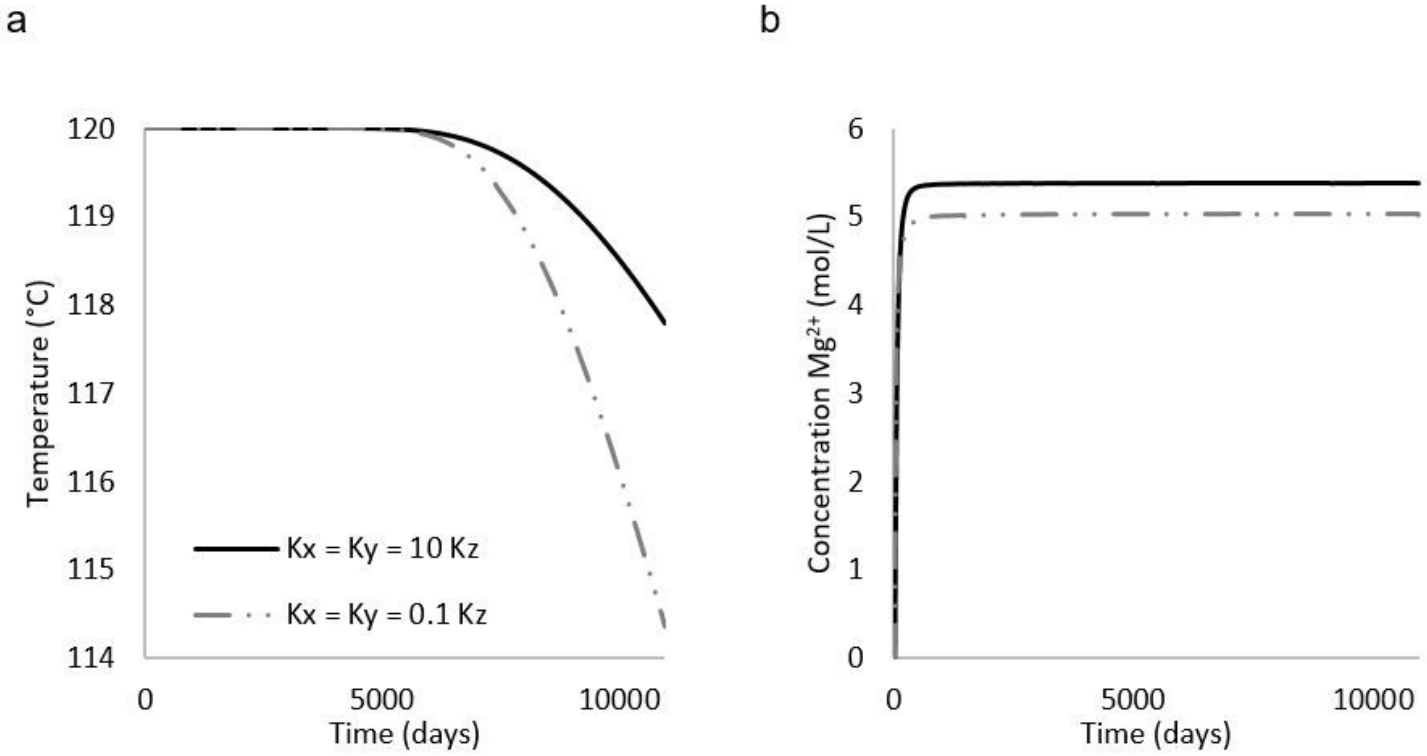

Figure 8

Comparison of sensitivity to anisotropy for a) observed temperature at the production well and b) Mg^{2+} at the production well in a geothermal doublet system.

Supplementary Files

This is a list of supplementary files associated with this preprint. Click to download.

- SupplementaryFiles.docx